JGR Earth Surface

RESEARCH ARTICLE
10.1029/2021JF006455

Key Points:

- We present a new method for rapidly quantifying baseline abrasion rate in the field via Schmidt Hammer Rock Strength
- Abrasion is extremely effective at this site due to vesicular volcanic rocks, yet easy to underestimate using simplistic sampling approaches
- We invoke transport-dependent abrasion to help explain the rapid downstream loss of the weakest grains

Supporting Information:

Supporting Information may be found in the online version of this article.

Correspondence to:

A. M. Pfeiffer,
pfeiffa@wwu.edu

Citation:

Pfeiffer, A. M., Morey, S., Karlsson, H. M., Fordham, E. M., & Montgomery, D. R. (2022). Survival of the strong and dense: Field evidence for rapid, transport-dependent bed material abrasion of heterogeneous source lithology. *Journal of Geophysical Research: Earth Surface*, *127*, e2021JF006455. https://doi.org/10.1029/2021JF006455

Received 30 SEP 2021
Accepted 19 MAY 2022

Survival of the Strong and Dense: Field Evidence for Rapid, Transport-Dependent Bed Material Abrasion of Heterogeneous Source Lithology

Allison M. Pfeiffer[1], Susannah Morey[2], Hannah M. Karlsson[2], Edward M. Fordham[1], and David R. Montgomery[2]

[1]Geology Department, Western Washington University, Bellingham, WA, USA, [2]Department of Earth and Space Sciences, University of Washington, Seattle, WA, USA

Abstract Bed material abrasion is a major control on the partitioning of basin-scale sediment fluxes between coarse and fine material. While abrasion is traditionally treated as an exponential function of transport distance and a lithology-specific abrasion coefficient, experimental studies have demonstrated greater complexity in the abrasion process: the rate of abrasion varies with clast angularity, transport rate, and grain size. Yet, few studies have attempted to assess the importance of these complexities in a field setting. Here, we develop a new method for rapidly quantifying baseline abrasion rate in the field via Schmidt Hammer Rock Strength. We use this method, along with measurements of gravel bar lithology, to quantify abrasion in the Suiattle River, a basin in the North Cascades of Washington State in which sediment supply to the channel is dominated by recurrent debris flows from a tributary draining Glacier Peak stratovolcano. Rapid downstream strengthening of river bar sediment and a preferential loss of weak, low-density vesicular volcanic clasts relative to non-vesicular ones suggest that abrasion is extremely effective in this system. The standard exponential model for downstream abrasion, using single-lithology abrasion rates fails to reproduce observed downstream patterns in lithology and clast strength. Incorporating heterogeneity in source material strength as well as transport rate-dependent abrasion largely resolves this failure. Further work is needed to develop a comprehensive quantitative framework for the dependence of bed material abrasion on grain size and transport rate.

Plain Language Summary As rocks transport along a riverbed, they hit one another and small pieces break off. This process is referred to as bed material abrasion. The rate of abrasion helps to control the ratio of sediment transported as gravel along the river bottom, and sediment transported in suspension (making the water turbid). In this study, we introduce a new method for estimating abrasion rate using a simple field measurement of rock strength. We then apply this method to the Suiattle River, which drains a stratovolcano that produces rock of varying strength. We use our field measurements to test the standard, simple mathematical approach for modeling bed material abrasion, and find it does a poor job of matching our field observations of how the riverbed rock mixture changes along the length of the channel. Finally, we test a more sophisticated model for abrasion that accounts for how rapidly grains transport. These model results better match our field observations, though we suggest that further work remains to improve models for bed material abrasion.

1. Introduction

Coarse sediment in transport along a riverbed gradually reduces in size as a result of grain-to-grain collisions (Daubrée, 1879). This process is termed abrasion and represents the combined effects of attrition, the gradual wear of the surface into fine particles, and fragmentation, the loss of larger particles (Attal & Lavé, 2009; Kuenen, 1956). Downstream abrasion is commonly modeled as an exponential decay of either the grain diameter or mass,

$$M_x = M_o e^{-\alpha x} \quad (1)$$

where M_o is the original grain mass, M_x is the grain mass at a given distance downstream, x is the downstream transport distance (commonly, in km), and α is a mass loss coefficient (1/km) representing abrasion rate (Sternberg, 1875). α is generally defined for a particular lithology either via laboratory experiments (e.g., Attal &

Lavé, 2009; O'Connor et al., 2014) or, in early studies, by observed downstream trends in bed material size (Adams, 1979; Bradley, 1970).

Bed material abrasion shapes both downstream fining and the partitioning of sediment flux between coarse and fine material. Much of the early work on bed material abrasion sought to explain the nearly ubiquitous trend of downstream fining of bed material. Half a century of research has demonstrated that both abrasion and transport processes can produce downstream fining. In the absence of abrasion, downstream fining can be explained by the concavity of river channels and modestly size-selective bed material transport (Ferguson et al., 1996; Hoey & Ferguson, 1994), as well as the evolution of river channels to accommodate increasing downstream sediment flux (Gasparini et al., 2004). While durable lithologies (for example., granite) lose mass too gradually to explain downstream fining in many rivers (Brierley & Hickin, 1991; Ferguson et al., 1996; Lewin & Brewer, 2002), abrasion of more friable lithologies is sufficient to explain the evolution of lithologic mixtures and grain size in other systems (Attal & Lavé, 2006).

Abrasion is an important control on the partitioning of basin-scale sediment fluxes between coarse and fine material. Durable, abrasion-resistant lithologies tend to be overrepresented in river beds relative to their proportion of the basin area (Attal & Lavé, 2006; Dingle et al., 2017; Mueller et al., 2016), while clasts of friable lithologies rapidly abrade, diminishing their fraction of the bed material (O'Connor et al., 2014) and producing silt and clay sized particles in the process (Attal & Lavé, 2009; Kodama, 1994). Through this control on coarse sediment flux, abrasion shapes downstream patterns in channel morphology. At the region-scale, O'Connor et al. (2014) found that the distribution of friable marine sedimentary bedrock in western Oregon, USA, strongly influenced the distribution of bedrock and alluvial channels, with mainstem bedrock channels found in basins lacking more durable source material.

While the classic Sternberg (1875) approach to modeling downstream abrasion (Equation 1) is still commonly employed (e.g., Mueller et al., 2016; O'Connor et al., 2014), its use has several recognized shortcomings. Experimental abrasion apparatuses fail to fully replicate bed material abrasion processes in the field. Barrel tumblers, the most common tool, likely underestimate the rate of abrasion in real rivers by overestimating the effective transport distance in the tumbler, and by failing to create realistic grain to grain impacts (Kodama, 1994; Lewin & Brewer, 2002). Abrasion is generally assumed constant for a given lithology, mapped geologic unit, or source material. Yet, several studies have noted that abrasion rate appears to decrease downstream. The weakest individual grains from a source area may abrade rapidly downstream from the source, preferentially strengthening the remaining coarse bed sediment (Attal & Lavé, 2006; Bradley, 1970; Dingle et al., 2017; Kuenen, 1956). This causes an apparent downstream decrease in the abrasion coefficient measured from bulk bed sediment (Adams, 1979; Sutherland et al., 2002). Adams (1979) documented this survivorship bias as reflected in a downstream increase in the ratio of abrasion-resistant quartzite pebbles initiating from sparse veins in source rock to pebbles made of the remainder of the source rock. While quartzite represents only a small fraction of the original source material, it can make up the majority of the bed material at sites tens of kilometers downstream. Clast weathering can also impact abrasion, with weathered grains of the same source lithology abrading many times faster than their unweathered counterparts (Bradley, 1970). In addition to the preferential survival of strong clasts, rapid abrasion downstream from a sediment source has been explained by efficient abrasion of corners of angular blocks of source material (Kuenen, 1956). Termed "Phase 1 abrasion" (Domokos et al., 2014), rapid mass loss during initial rounding, followed by more gradual abrasion of rounded particles ("Phase 2"), has been demonstrated in both models and laboratory experiments (Domokos et al., 2014), and observed in the field (Miller et al., 2014). Furthermore, Equation 1 frames abrasion as a function of transport distance, yet immobile grains are subject to collisions with passing mobile particles (Prancevic et al., 2020) and while jostling in the flow (Schumm & Stevens, 1973), and thus almost certainly abrade in place. This immobile-grain abrasion process may be particularly important in coarse headwater streams where both large, immobile boulders and mobile gravel bed material are common. Finally, in Equation 1 abrasion does not vary with the intensity of sediment transport. Both tumbling mill (Kuenen, 1956) and circular flume experiments (Attal & Lavé, 2009) reveal that abrasion increases with particle transport velocity (a phenomenon herein referred to as transport-dependent abrasion).

This study builds on previous research in two ways: by explicitly considering the role of variability in sediment strength within a single mapped geologic unit, and by accounting for transport-dependent abrasion in our model for the downstream evolution of coarse sediment. Models of downstream abrasion have generally relied on laboratory experiments using bulk sediment mixtures taken in the field to estimate the abrasion potential of

a given sediment source. Such labor-intensive methods limit the feasibility of characterizing variability in sediment abrasion rates within a given source area. We hypothesize that this variability acts as an important control on the downstream evolution of sediment in a basin. To overcome this limitation, we develop a new method for rapidly quantifying tumbler-derived bed material abrasion rate in the field via Schmidt Hammer Rock Strength (SHRS). We use this new method, along with measurements of gravel bar lithology, to quantify abrasion along the Suiattle River, a basin in the North Cascades of Washington State dominated by a localized coarse sediment source: recurrent, debris flows from a small tributary draining Glacier Peak stratovolcano. While the dependence of bed material abrasion on sediment transport rate (rather than just transport distance) has been demonstrated in the lab (Attal & Lavé, 2009), to our knowledge, no studies have attempted to either model or corroborate this phenomenon with field observations. Here, we use our detailed observations of source material grain strength, density, and size to model downstream transport-dependent abrasion. This study is made feasible by two particular characteristics of this field site: sediment supply is dominated by a localized source, and the supplied sediment consists of heterogeneous volcanic tephra including vesicular and non-vesicular clasts that abrade and transport at different rates.

In this paper we begin by establishing a method for characterizing bed material abrasion potential, as measured by tumbling experiments, via SHRS. Then, we use this method to explore the relationship between source material characteristics and downstream trends in gravel bar lithology and rock strength in the Suiattle River basin. Finally, we apply existing models (Attal & Lavé, 2009; Sternberg, 1875) for bed material abrasion to the case of the Suiattle and compare them to the observed downstream trends.

2. A Method to Characterize Abrasion Potential via SHRS

Bed material abrasion rate, α (Equation 1), is typically determined in laboratory experiments using either cylindrical rotating drums (e.g., Kodama, 1994; Kuenen, 1956; O'Connor et al., 2014) or annular flumes (Attal et al., 2006). These approaches are time consuming, with tumbling times of hours to days for each sample. Furthermore, rock samples must be transported to the lab. This poses an additional challenge for remote field studies interested in characterizing the abrasion potential of multiple sediment sources. To overcome these challenges, here we present a relationship between in-situ SHRS and laboratory-determined bed material abrasion rate (α_t).

SHRS has been used as a proxy for abrasion potential in geomorphology studies focused on bedrock river incision processes (Duvall et al., 2004; Murphy et al., 2016), as well as engineering studies focused on the abrasion of dry rock aggregate for construction (Kahraman & Gunaydin, 2007) and as a proxy for bed material abrasion potential (Miller et al., 2014). We sampled SHRS of large cobbles and small boulders along the Suiattle River, making $\geq$10 measurements on each boulder, distributed evenly across smooth surfaces of the clast using a Proceq Rock Schmidt to capture any variability in strength within the clast due to fractures, orientation of measurement relative to metamorphic fabric or sedimentary bedding planes, or other source of spatial heterogeneity (Bernard et al., 2019). Here, and elsewhere in this paper, reported SHRS values refer to the median of 10+ measurements on a given clast. Reliable measurements of SHRS must be made on samples greater than 11 cm in diameter (Demirdag et al., 2009). However, >11 cm clasts are prohibitively large for tumbler experiments. To overcome this issue, we extracted 2–4 smaller subset clasts for tumbling from the large measured grains, either by rock saw in the lab, or by rock hammer in the field.

We conducted tumbling experiments to measure the rate of mass loss of individual particles during fluvial transport. Cutting or breaking the sample grains from their original boulders yielded irregularly shaped clasts. Because irregular grains abrade more rapidly than rounded particles (Domokos et al., 2014), we conducted an initial phase of tumbling of each clast until all sharp edges were worn away. Using a tumbling setup similar to that of O'Connor et al. (2014), we filled a rock tumbler with 2.5 kg of sediment and 2 L of water. Each experimental run consisted of a "host" grain size distribution (GSD) similar to that of gravel patches along the lower mainstem of the Suiattle. The "sample" particles were always a different lithology from the host distribution. For example, plutonic sample particles were tumbled in a host distribution of volcanic sediment. This allowed us to easily distinguish sample particles from the host distribution, and better mimics the mixed-lithology abrasion conditions present in the field. 4–8 sample clasts were included in each run. Sample clasts were grouped to be easily

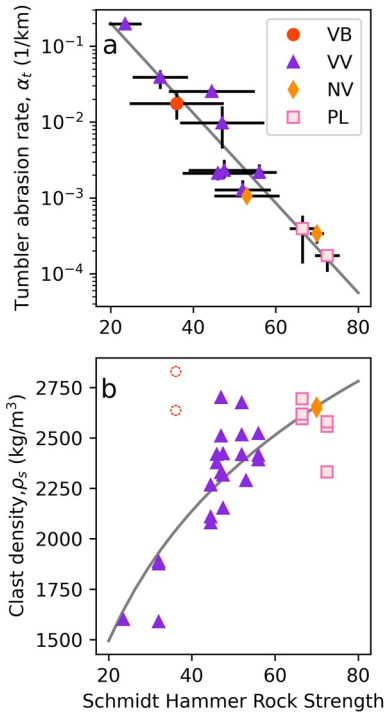

Figure 1. Measured relationship between Schmidt Hammer Rock Strength (SHRS) and (a) tumbler-derived abrasion rate and (b) wetted-clast density. Horizontal error bars in panel (a) denote the standard deviation of 10+ individual SHRS measurements on a single boulder, while vertical error bars mark the minimum and maximum measured abrasion rate for the 2–4 subset clasts extracted from the boulder. All markers colored by clast lithology. VB = volcanic breccia, VV = vesicular volcanics, NV = non-vesicular volcanics, PL = plutonic. Points in figure (b) mark the measured density of individual clasts. The dotted circles denote volcanic breccia samples, which were excluded as outliers from the regression.

distinguishable by color, size, and shape even if inked sample number labels wore off during a round of tumbling. Starting sample grain mass ranged from 5 to 430 g, with a mean of 126 g.

At the start of each sampling run, we submerged the sample grains in water for 48 hr to allow void spaces to fill with water. We towel-dried and weighed each sample clast, tumbled the grains for 2–20 hr, then dried and weighed them again. Following O'Connor et al. (2014), we converted tumbler experimental time to transport distance using the tumbler revolution rate and inner circumference of the tumbling barrel, yielding a conversion of 1 hr–1.15 km of transport. The total duration of tumbling varied with sample strength. We repeated this process until >2% of the original clast mass had abraded, or for at least 50 km of simulated transport. For each clast, we used a best fit regression to calculate the tumbler-derived mass loss coefficient, α_t.

Laboratory methods for quantifying bed material abrasion rate have received criticism (see Lewin & Brewer, 2002) for systematic underestimation of abrasion rates in real rivers. Barrels tend to yield underestimates of bed material abrasion rates, perhaps by a factor of 2–3 or more (Lewin & Brewer, 2002). The underestimate of tumbler-derived abrasion rates may be due to low particle impact velocities relative to transport in natural channels and/or the assumption that the barrel circumference and rotation rate can be used as a proxy for particle transport distance. To correct for this, we explore the use of a tumbler correction factor below.

Our new method for characterizing α_t via SHRS proves highly effective. In our tumbling experiments, individual clast abrasion rate is well fit by exponential decay, conforming with the classic Sternberg expression (Equation 1) for bed material abrasion (Figure S1 in Supporting Infomation S1). Comparing these experimentally determined clast abrasion rates to measured SHRS, we find a strong relationship (Figure 1a). The range of SHRS and abrasion rate sampled here encompasses much of the range of both parameters in natural rocks (Attal & Lavé, 2009; Demirdag et al., 2009).

In addition to measuring abrasion rate, we quantified clast density for each tumbled grain by measuring the volume, to the nearest mL, of each sample clast via displacement of water. Clast density is needed for our transport-dependent abrasion calculations (see below). As with abrasion rate, we use SHRS as a proxy for density. We find that clast density varies systematically with SHRS for all but the sample clasts of volcanic breccia (Figure 1). Volcanic breccia makes up a very small portion of the bed material in the Suiattle. The volcanic breccia boulder sampled for use in the tumbling experiments was characterized by a low density vesicular matrix surrounding high density angular clasts. Our SHRS measurements were made on a boulder in the field, and included measurements centered on both matrix and clast material. Because our density measurements were made after the tumbling experiments were complete, we suspect that the ratio of matrix and clast material had decreased, yielding a grain that increased in density over the course of tumbling. As a result of the heterogeneous density, that likely differs from the density of the original boulder when SHRS measurements were made, we exclude the volcanic breccia from our SHRS-density regression.

This proxy for the abrasion potential of bed material clasts establishes a new method with which we can test existing models for bed material abrasion. In addition to simply quantifying the relative proportions of different rock types at a variety of sites in a basin or region, we can now make quantitative measurements of the distribution of α_t, both at the source and in the bed material downstream.

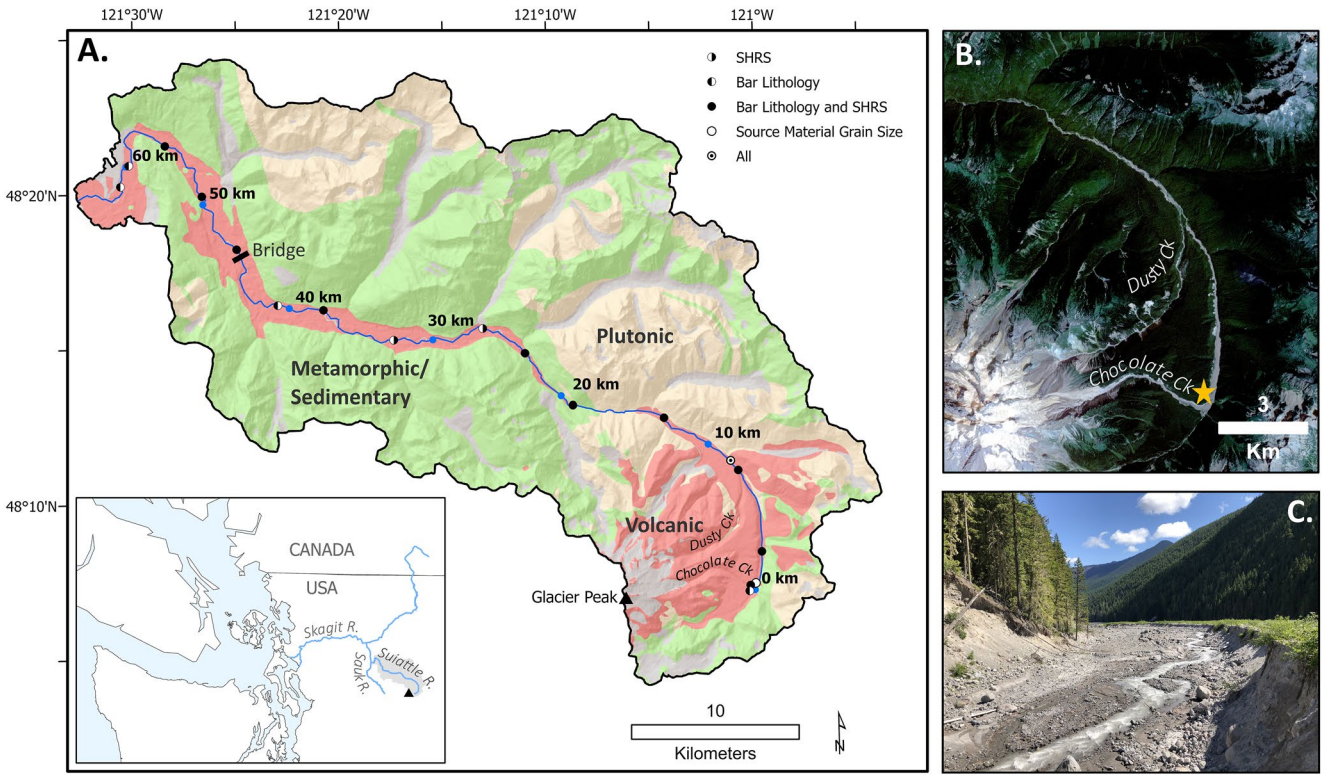

Figure 2. Field Site. (a) Simplified geologic map of the Suiattle basin with field measurement sites marked according to the type of data collected. Downstream distance from Chocolate Creek (CC) debris flow deposit marked in blue dots. Other lithologies including ice, alluvium, and ice sheet deposits shown in gray. (b) Satellite imagery of the upper 15 km of the basin (Planet Imagery). (c) Source material debris flow terraces along CC, photo taken at location marked by the star in (b).

3. The Suiattle: Downstream Changes in Material Strength and Lithology

3.1. Field Site

The Suiattle River drains the eastern flank of Glacier Peak, an active stratovolcano in the North Cascade Mountains of Washington State, USA (Figure 2). The upper Suiattle River falls within the Glacier Peak Wilderness Area, an area with minimal human impact. There are no dams or sediment control structures in the Suiattle basin, and few roads.

Normalized for drainage area, the Suiattle basin contributes about twice as much suspended sediment to the lowland as typical stratovolcano basins in the Pacific Northwest, including those on the west side of Glacier Peak (Czuba et al., 2011; Jaeger et al., 2017). This anomalous sediment load has been attributed to Chocolate Creek (CC) (Jaeger et al., 2017), a small tributary rapidly incising a Holocene volcanic apron of lahar and pyroclastic flow material (Beget, 1982). Large mid-to late-20th century debris flows deposited a >3 m thick, 0.5 km wide fan of unconsolidated volcanic material at the confluence of CC and the Suiattle River (Ford, 1959; Slaughter, 2004). This debris flow material provides a large, localized source of volcanic sediment high in the watershed, augmented by lesser debris flow contributions from Dusty Creek, the next tributary downstream (Beget, 1982).

The dominance of the eastern flank of Glacier Peak in the sediment budget of the Suiattle has been inferred by many researchers working in the basin (Beget, 1982; Ford, 1959; Slaughter, 2004), likely due to the sparsely vegetated valley bottom (visible as a bright strip in the aerial imagery in Figure 2b) that extends from CC into the mainstem Suiattle and tapers out where the Suiattle enters a bedrock canyon 16 km downstream. Sediment-related datasets are sparse, however, and no bedload transport data exist to directly quantify the coarse sediment load of the Suiattle and its tributaries. Quantitative constraints on the large magnitude of sediment contributed by Chocolate, and potentially Dusty Creeks (each <1% of the Suiattle basin area), comes from two recent studies. Using a 5-year record of suspended sediment measurements along the Sauk River and estimates of "background"

sediment yields from neighboring basins, Jaeger et al. (2017) estimate that 61% of the suspended sediment yield in the Suiattle comes from "pro-glacial point sources" on the eastern flank of Glacier Peak. Further support comes from work on channel-adjacent lahar and glacial terrace bluff erosion (Scott & Collins, 2021) in the Suiattle (lower valley bottom volcanics, shown in Figure 2a). While sediment contributions from channel-adjacent bluffs of mid-Holocene lahar and Cordilleran Ice Sheet sediments are responsible for a median of 24% of the sediment yield in rivers in the region, data from Scott and Collins (2021) suggest that they account for only 6% of the sediment budget in the Suiattle. Given that the Suiattle has a remarkably high sediment load, the findings of Scott and Collins (2021) are consistent with a Suiattle sediment budget dominated by non-bluff sources.

The debris flow fan at CC represents a regularly replenished sediment source that has been active for sufficient time for the downstream bed to have adjusted. Large debris flows from CC initiated around 1938 (Slaughter, 2004). Debris flows of varying magnitudes have recurred in the decades since, reported in eyewitness accounts (Richardson, 1968), and documented in historical aerial imagery (Slaughter, 2004) and anomalous suspended sediment spikes at gauges downstream (Jaeger et al., 2017). These recurring events have regularly replenished the deposits of material available for fluvial transport in the channel. Studies of sediment pulse transport in similar mountain rivers in the region suggest that sufficient time has passed for this debris flow sediment to transport the full length of the Suiattle. In one nearby channel, a wave of aggradation has passed downstream at a rate of 1–4 km/year (Anderson & Konrad, 2019). Similarly, a post dam removal study nearby found that the majority of reservoir sediment had transported the 18 km downstream to the ocean within just two years of dam removal (East et al., 2015). Thus, in the subsequent analysis of downstream patterns in lithology and rock strength in the Suiattle we assume that the volcanic sediment sourced from CC represents a steady state condition of reworked and abraded material.

3.2. Field Methods

In this section, we quantify the sedimentary characteristics of the Chocolate and Dusty Creek source material, then quantify downstream trends in bed material lithology and rock strength throughout the channel.

3.2.1. Field Measurements of Source Material

We measured the GSD of the debris flow source material in freshly exposed, sub-vertical terraces along CC and the mainstem Suiattle at the Chocolate and Dusty confluences. These terrace exposures were cleaned of loose colluvium to expose a fresh, undisturbed cross section. We measured grains in a 20 cm grid, defined by tape measures hung from the top of the terrace tread. Selected grains were removed from the deposit, and their intermediate axis was measured to the nearest 5 mm. Grains smaller than 5 mm were binned into a single size class. We estimated the intermediate axis diameter of grains that were too large to safely remove, based on their exposed dimensions. The largest grains were occasionally encountered more than once along the grid. These grain diameters were recorded multiple times to account for their abundance in the GSD. At each of the 5 sites we measured the diameter of 50–100 grains, for a total of >350 measured grains (Bunte & Abt, 2001). To characterize the abrasion rate (α) of grains in the deposit, we measured the SHRS of 100 grains of diameter >11 cm within, or in the undisturbed colluvium directly below, fresh terrace faces. These 100 clasts include all sufficiently sized clasts encountered during the gridded clast count (described above). If we failed to encounter 100 sufficiently large clasts during the gridded clast count, we randomly selected clasts in the colluvium at the base of the terrace until 100 measurements were reached.

3.2.2. Quantifying Downstream Trends in Grain Size, Lithology, and Bed Material Strength

To characterize the rate of bed material abrasion in the Suiattle, we quantify downstream trends in bed surface grain size, SHRS, and lithology on exposed gravel bars along the Suiattle River between the headwaters and the confluence with the Sauk River (Figure 2).

We measured SHRS and recorded the lithology of ≥50 boulders at 15 sites along the length of the Suiattle (Figure 2). All measured grains had a diameter of >11 cm along their smallest axis (the limit for size-independent SHRS measurements, as noted above). We measured clasts at several randomly selected locations spread across each gravel bar, measuring all sufficiently sized clasts within reach of that point. We classified the lithology of

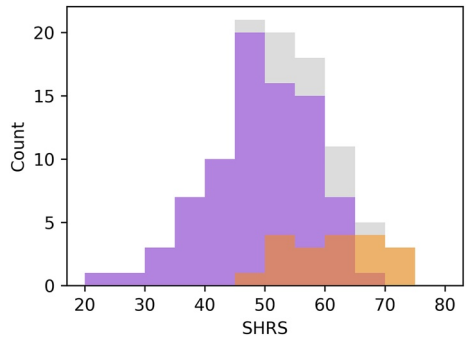

Figure 3. Distribution of measured clast strength within the source deposit, which is entirely volcanic. All clasts shown in gray, vesicular volcanics in purple, non-vesicular volcanics in orange.

each boulder as vesicular volcanic, non-vesicular volcanic, volcanic breccia, metamorphic/sedimentary, or plutonic.

In addition to the boulder strength measurements, we quantified bar surface grain size and lithology at 13 sites along the channel. At each site 200 grains were blindly selected from the bar surface every two steps along repeated transects across the width of the exposed bar. Intermediate axis dimension was measured to the nearest cm. Because many large boulders were partially buried, we measured the diameter of their smallest exposed axis as a proxy for the intermediate grain axis. The lithology of each grain was classified using the categories described above. In our measurements, we excluded fine particles less than 1 cm in diameter, which were too small to reliably classify in the field. A small number of measured particles (<1% of all grains measured) were deemed unclassifiable due to their small size. Note that measurements of bar material lithology were made at many, but not all, of the same sites as our SHRS measurements (Figure 2) due to logistical constraints of the remote setting.

3.3. Suiattle Field Data Results and Discussion

Debris flow deposits in the upper Suiattle are poorly sorted mixtures ranging in size from silt to large boulders (Figure S2 in Supporting Information S1). Combining measurements from our 5 sites, the D_{50} of the coarse material (i.e., >2 mm) is 90 mm, with individual site D_{50} between 75 and 120 mm. Fine (<2 mm) sediment makes up approximately 22% of the deposit. The largest measured grains are 1.3 m, though we note that boulders up to 5 m in diameter can be found scattered throughout the deposit.

The strength (SHRS) of source material boulders varies substantially, from 24 to 73.5, with a mean of 51 (Figure 3). Using our calibration curve, this yields a mean tumbler-derived abrasion rate of 0.3% mass loss per kilometer. Among the measured source material boulders, 81% were vesicular volcanics, and the remaining 19% were non-vesicular volcanics. The vesicular volcanic clasts were systematically weaker than their non-vesicular counterparts, with SHRS between 24 and 65, compared to a range of 47–73. This wide range in the strength of volcanic rock is consistent with previous work on rock strength in volcanic sedimentary systems (Huddart, 1994; O'Connor et al., 2014).

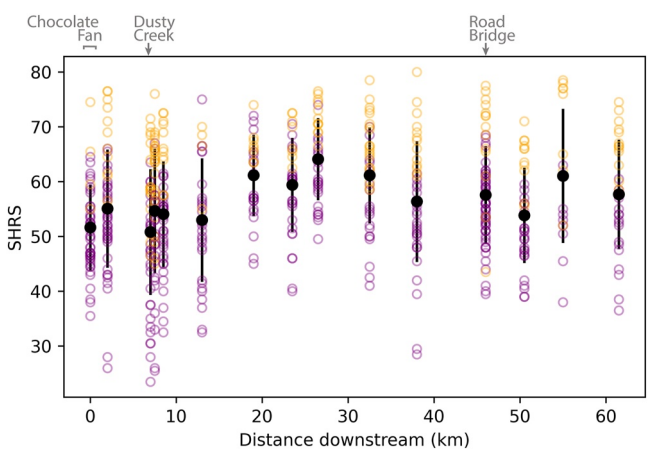

Figure 4. Measured Schmidt Hammer Rock Strength (SHRS) of volcanic clasts on river bars along the Suiattle. Hollow circles represent the SHRS of individual clasts (value shown is the median of 10 measurements made on each clast), with vesicular volcanics in purple and non-vesicular in orange. The mean SHRS of all measured clasts on that gravel bar are marked in black. Black lines mark the standard deviation.

In the channel, mean boulder SHRS increases rapidly over the first 25 km downstream from the source, followed by roughly stable boulder strength in the lower portion of the channel (Figure 4). The rapid downstream strengthening of boulders coincides with an increase in the minimum measured SHRS, but little change in the maximum measured SHRS of boulders.

Upstream from the debris flow source zone volcanic clasts make up less than half of the measured grains on the gravel bar (Figure 5). Where the Suiattle incises historic debris flow terraces, the lithology of the gravel bars is dominated by volcanic rocks (95%). Both the fraction of volcanic sediment and the ratio of vesicular to non-vesicular volcanics decrease rapidly in the 20 km immediately downstream from the Chocolate Fan. In the lower 40 km, trends in the volcanic fraction and ratio of vesicular to non-vesicular grains are more subtle. The ratio of vesicular to non-vesicular volcanics varies between 0.8 and 1.6 between 23 and 46 km. In the lower 10 km of the channel, the ratio of vesicular to non-vesicular volcanics drops and the overall proportion of volcanics decreases, coinciding with a larger portion of plutonic and metasedimentary bed material. The location of this increase in plutonic and sedimentary sediment lies just 2 km upstream of the first terrace-top exposure of the Cordilleran Ice Sheet deposits, mapped in gray in Figure 2a on river right starting at kilometer 57. Given that the Cordilleran Ice Sheet deposits (~17

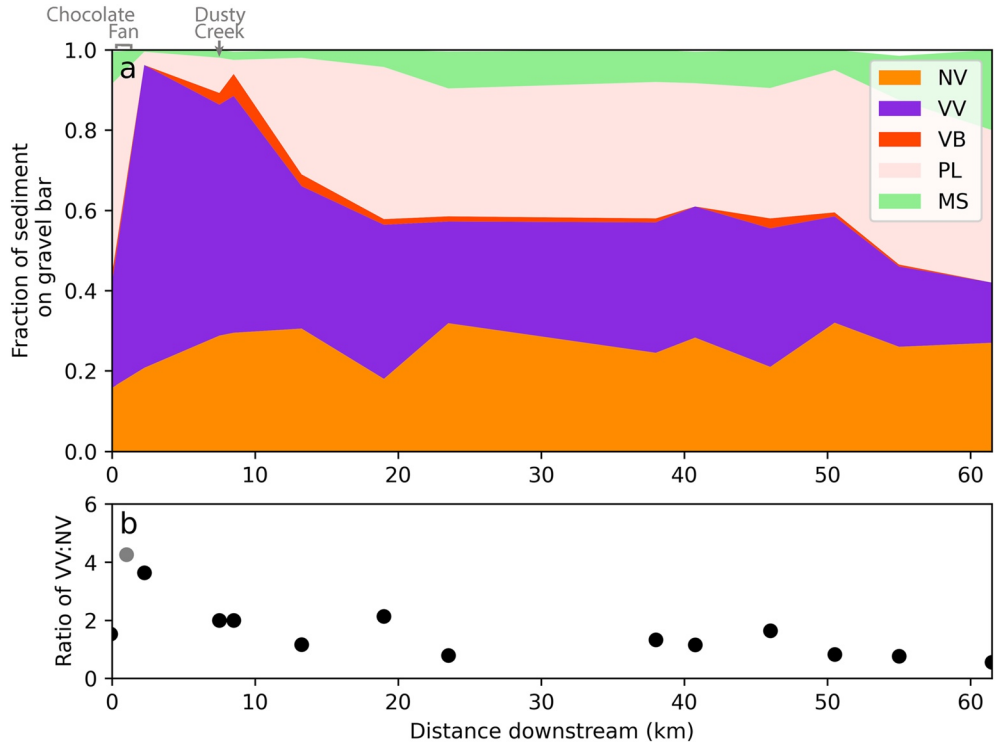

Figure 5. Downstream trends in gravel bar lithology along the Suiattle. (a) Proportions of each lithology category at each downstream site. NV = non-vesicular volcanics, VV = vesicular volcanics, VB = volcanic breccia, PL = Granite and other plutonic rocks, MS = metamorphic and (meta) sedimentary. Unclassified lithologies shown in white, at the top of the stacked plot. (b) Ratio of vesicular to non-vesicular volcanics with distance downstream. Gray dot denotes the VV:NV ratio of the source material.

kyr) lie stratigraphically below the lahars (~5.5 kyr), they are likely exposed in, and rapidly eroding from (Scott & Collins, 2021) the channel-adjacent bluffs, acting as a local source of non-volcanic sediment supply.

As a check of consistency in our measurements, we can compare the SHRS of volcanic boulders and lithology of bar sediment at the first site incising the CC fan with the SHRS and lithology of boulders in the source deposit. We find good agreement in both mean SHRS (both 51) and the percentage of vesicular volcanics (75% versus. 81%). The consistency between source and channel lends support to our assertion that sediment from the CC fan dominates sediment supply at this location.

Downstream patterns in gravel bar lithology (Figure 5), combined with the rapid loss of weak grains inferred from the downstream patterns in SHRS (Figure 4), suggest that abrasion processes are extremely effective in the Suiattle River. The abrupt increase in the proportion of volcanic grains at the CC Fan (Figure 5), from 42% just upstream to 96% at the first site downstream of the introduction of debris flow material, supports our assertion that these debris flow deposits represent a dominant source of sediment in the upper basin. This increase in volcanics in the bed material is associated with negligible change in the fraction of upstream basin area mapped as volcanic (32% upstream of Chocolate Fan to 37% at the fan, Figure S3 in Supporting Information S1). The loss of weak vesicular volcanics in the subsequent 19 km is particularly rapid downstream from Dusty Creek. Downstream of this zone of rapid loss of volcanics there is stabilization of the relative lithologic proportions, suggesting that while abrasion processes are extremely effective upstream, their effects diminish with downstream distance from the source. The rapid change cannot be easily explained by tributary sediment input. In the 19 km downstream of Chocolate Fan, the proportion of volcanic bed material decreases from 96% to 66%. Over this distance, the upstream proportion of the basin mapped as volcanics decreases minimally: from 37% to 34% (Figure S3 in Supporting Information S1). Furthermore, dilution of the volcanic fraction by tributary or landsliding inputs would result in a change in the fraction of both vesicular and non-vesicular clasts. Instead, we see

a loss in vesicular grains but little change in the proportion of non-vesicular volcanics. This supports abrasion as the driver of the change, rather than inputs.

4. Modeling Abrasion of the Volcanic Source Material

4.1. Sternberg Abrasion Model

To quantify the abrasion potential of the CC volcanic sediment, we predict volumetric loss of the coarse source material to wash load over 65 km of transport. We begin by using a simple Sternberg (1875) exponential model for mass loss of coarse source material from the bed surface with transport distance (Equation 1). We calculate tumbler-based abrasion rates from the measured distribution of source material SHRS (Figure 3) using the best fit regression between SHRS and α_t in Figure 1a. To account for the fact that barrel tumblers likely underestimate the rate of abrasion in real rivers (Kodama, 1994; Lewin & Brewer, 2002), we explore the effect of incorporating a tumbler correction factor (C_t), where the baseline abrasion rate used in Equation 1 is:

$$\alpha_{\text{baseline}} = C_t \alpha_t \tag{2}$$

While previous work suggests that C_t should be greater than one, the literature does not provide us tight constraints on values for these parameters. Lewin and Brewer (2002) found that tank-derived abrasion rates were higher than tumbler-derived abrasion rates by a factor of roughly 2–4 for the same sediment, though the abrasion rates of individual natural clasts within an experiment varied by more than an order of magnitude.

The top row in Figure 6 (panels a, b, and c) shows the resulting predicted coarse material volumetric loss. In the case of no tumbler correction factor (Figure 6a), the total volumetric loss of coarse material to products of abrasion is modest. Incorporating a tumbler correction factor of 4, which is at the upper end of what is supported by previous experiments (Lewin & Brewer, 2002), yields gradual downstream abrasion of the volcanic source material (Figure 6c) and a total loss of 53% of the original coarse material over 65 km of transport.

4.2. Transport-Stage Dependent Abrasion Model

While Sternberg (1875) remains the standard approach for modeling downstream bed material abrasion, Attal and Lavé (2009) showed that for a given lithology, abrasion rate increases with pebble transport velocity (u_p) at high velocities. According to Sklar and Dietrich (2004):

$$u_p \propto \left(\frac{\rho_s - \rho_w}{\rho_w} D \left(\frac{\tau^*}{\tau_c^*} - 1 \right) \right)^{0.5} \tag{3}$$

where ρ_s is sediment density, ρ_w is water density, D is grain diameter (in meters), τ^*_c is the dimensionless critical bed shear stress associated with the threshold for grain motion, and τ^* is the dimensionless bed shear stress for a given particle at a given flow, calculated as

$$\tau^* = \frac{\tau}{(\rho_s - \rho_w) g D} \tag{4}$$

with τ^*/τ_{*c} often referred to as transport stage. Based on their finding that abrasion rate scales with u_p^2, Attal and Lavé (2009) propose that

$$\alpha \propto \frac{\rho_s - \rho_w}{\rho_w} D \left(\frac{\tau^*}{\tau_c^*} - 1 \right) \tag{5}$$

In Equation 5, we have retained the densities from Equation 3, which Attal and Lavé (2009) take as constants. They suggest that at lower transport stages ($\tau^*/\tau_{*c} < \sim 3.3$), particle mass loss is higher than this transport-dependent curve due to mobile grains impacting immobile grains on the bed (Figure 7a).

The Attal and Lavé (2009) experiments yielded a "semi-schematic diagram" describing this relationship between transport stage and abrasion rate (Figure 7a). Here, we use this diagram and Equation 5 to inform a simple equation for transport-dependent bed material abrasion, which is represented graphically in Figure 7b. We assume that each grain has a baseline abrasion rate (α_{baseline}) set by its strength, which we calculate from SHRS using the

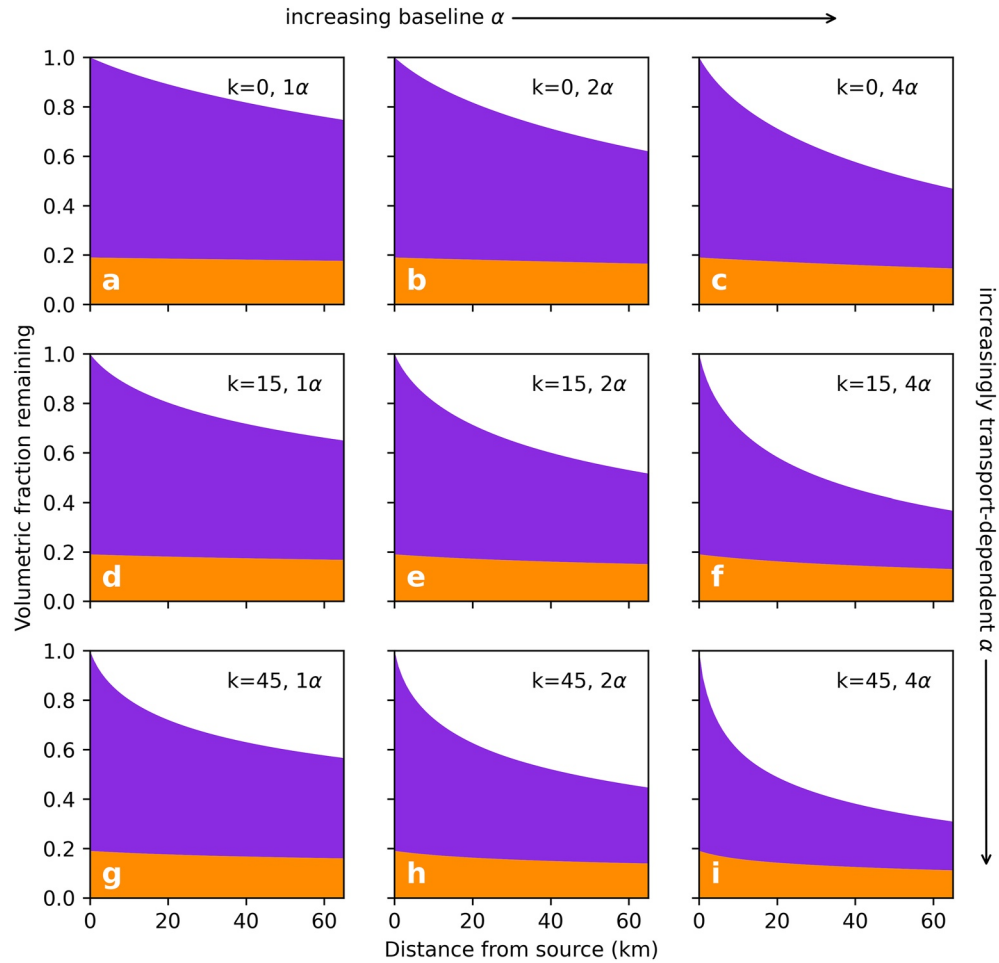

Figure 6. Modeled abrasion of Chocolate Fan sediment (not including incorporating other sediment sources) over 65 km of downstream transport assuming a variety of transport dependence (k) and tumbler abrasion correction values. Vesicular volcanics are shown in purple, non-vesicular in orange, while the products of abrasion (material lost to wash load) are shown in white.

best-fit regression in Figure 1a, multiplied by a tumbler correction factor, C_t, as in Equation 2, above. At transport stage (τ^*/τ_{*c}) > 3.3, the abrasion rate of a grain increases above this baseline value (Figure 7b):

$$\alpha = \alpha_{baseline}\left(1 + k\frac{\rho_s - \rho_w}{\rho_w} D\left(\frac{\tau^*}{\tau_c^*} - 3.3\right)\right) \quad (6)$$

where k is a coefficient that determines the degree of transport-dependence. A k value of 15 approximates the slope of the transport-dependent abrasion relationship described by Attal and Lavé (2009). We discuss our choice of k in the below. For transport stage less than or equal to 3.3, the abrasion rate remains at the baseline value.

Predicting downstream sediment abrasion using Equation 6 requires us to define an initial GSD of the sediment as well as downstream flow characteristics. We represent sediment as "parcels" of bed material (*sensu* Czuba, 2018; see Section 5.1, below) of uniform initial volume and grain size, with each parcel's grain size randomly selected from the measured CC source material GSD. In doing so, we assume that GSD does not vary systematically with lithology.

To assign a transport rate for each parcel of sediment at each downstream point in the channel, we must first assign τ^*. Rather than specifying a particular channel profile and representative flow depth (used to determine τ), or creating a full morphodynamic model that would represent both selective transport and abrasion, we take

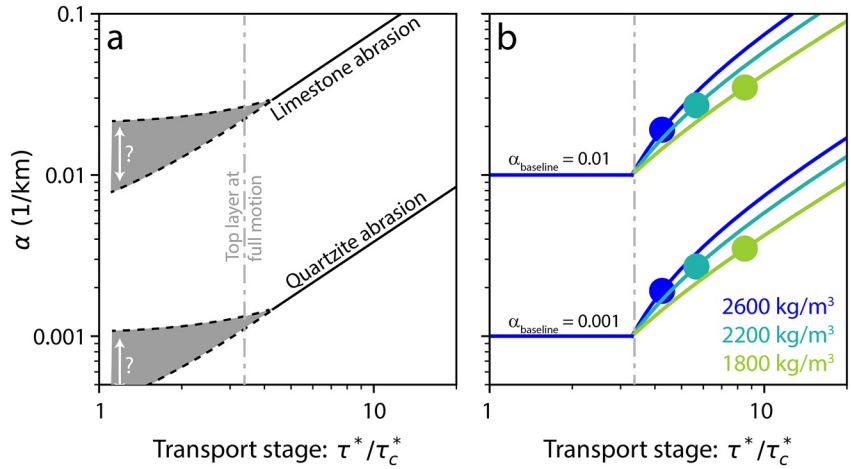

Figure 7. (a) "Semi-schematic" model of transport-dependent bed material abrasion, modified from Attal and Lavé (2009). (b) Representation of transport-dependent bed material abrasion used in this paper (Equation 6), demonstrating the effect of clast density on abrasion rate. Curves are colored by clast density. Dots represent calculated abrasion rates for 40 mm grains of three different densities in a 120 Pa flow, $k = 15$, $\tau^*_c = 0.045$.

a simplified approach. The median surface grain size on the upstream most channel bar is 0.14 m. We assume exponential downstream fining in a river channel with a diameter loss coefficient (δ) of 0.01:

$$D_{x50} = D_{o50}e^{-\delta x} \tag{7}$$

where D_{x50} is the median grain size at a given distance (x) downstream, and D_{o50} is the starting median grain size, in this Case 0.14 m. This approach, and choice of δ, yields downstream patterns that approximately match the fining trends we see in the Suiattle (Figure S4 in Supporting Information S1), decreasing from a D_{50} of 0.14 m at CC to 0.08 m 62 km downstream, near the confluence with the Sauk. For each downstream distance in the channel, we assume a representative shear stress twice that required to transport D_{x50} (Pfeiffer et al., 2017) of mean sediment density (calculated based on the source material):

$$\tau_x = 2\tau^*_c \left(\overline{\rho_s} - \rho_w\right) g D_{x50} \tag{8}$$

where we assume $\tau_{*c} = 0.045$, water density $\rho = 1000$ kg/m^3, g = 9.81 m/s^2. This yields plausible dimensional shear stresses of 160 to 37 Pa (Figure S4b in Supporting Information S1). Our results are not particularly sensitive to the choice of representative shear stress (Figure S5 in Supporting Information S1), nor are they sensitive to uniform shifts in the grain size in Equation 7 (Figure S6 in Supporting Information S1). However, the results do vary dramatically if we assume a uniform grain size, rather than using the wide observed GSD (Figure S6 in Supporting Information S1).

We calculate parcel-specific mass loss at each downstream distance from Equation 6 and Equation 1, assuming a baseline α and parcel density for each parcel based on SHRS, as above. From parcel-specific mass loss, we calculate downstream changes in parcel volume (V) and grain size (D):

$$D_x = D_{x-dx}\left(\frac{V_x}{V_{x-dx}}\right)^{1/3} \tag{9}$$

If any parcel abrades to a grain diameter smaller than gravel (<0.002 m), we consider it a "product of abrasion" and remove it from subsequent downstream abrasion calculations.

In these abrasion calculations, we make several implicit assumptions. First, we assume that the CC sediment is added to the channel at a single point. To the extent that these calculations are intended to model abrasion of volcanic sediment in the Suiattle, we believe this is a reasonable simplification. Historical accounts and field evidence suggest that CC dominates sediment contributions to the channel, with Dusty Creek (7 km downstream) as a secondary source of occasional volcanic debris flows (Figures 2a and 2b). A second assumption

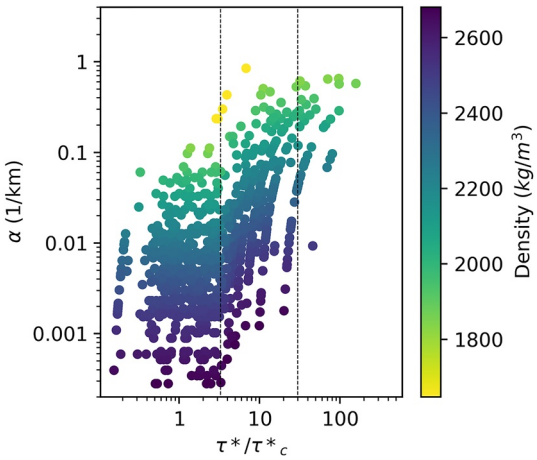

Figure 8. Calculated transport stage and abrasion rates for 1,000 parcels of sediment representing the source material grain size, rock strength, and density distributions, and assuming $k = 15$ and a tumbler correction factor of two at a distance 10 km downstream from the source.

in these calculations is that the full GSD of the source material transports downstream, rather than the coarsest grains remaining as a lag deposit in the upper reaches of the channel. While there are large boulders within the debris flow terraces, the bed of the Suiattle is not dominated by these boulders (Figure 2c), suggesting that coarse sediment does not remain at the source as a lag deposit. A third assumption relates to the products of abrasion. Abrasion represents the combined effects of attrition, which produced clay, silt, and sand sized grains, and fragmentation, which produces larger grains (Kodama, 1994). Here, we assume that the products of abrasion "disappear" from the bed material. Abrasion can produce both fine (silt and sand) particles and fragments. In the Suiattle, these fine particles would transport in suspension. While the fragments can be larger, they tend to be angular. Angular particle abrasion is many times higher than rounded particle abrasion. Furthermore, the fragments tend to be small relative to the coarse GSD of this channel (Attal & Lavé, 2009), and would thus have high transport rates in subsequent downstream transport, further increasing their rapid transformation to suspended load. Finally, in these calculations, we do not include "Phase 1" abrasion (Domokos et al., 2014) of angular clasts into rounded ones. Clasts in the debris flow terraces are subrounded, which helps to justify this omission.

Our transport-dependent abrasion model suggests that while $\alpha_{baseline}$ varies by 3 orders of magnitude in the Suiattle, in the case of $k = 15$, transport-dependent increases in abrasion are responsible for a ~1 order of magnitude increase in α (Figure 8). Rapid transport of grains gives a modest boost to the effectiveness of abrasion, though baseline abrasion rate remains the first order control on α. Because SHRS varies with both abrasion rate and clast density, the weakest grains in our transport model are also the most mobile when normalized for grain size. The small and low density grains are most prone to enhanced, transport-dependent abrasion. Of these highly mobile, high predicted α grains, a small number have transport stages >30 (Figure 8), suggesting that they are transporting in suspension, rarely contacting the bed (Sklar & Dietrich, 2004). In reality, the low frequency of bed contact likely results in a decreased abrasion rate, at least in that stretch of channel. However, our focus in this paper is on the downstream loss of bed material, making unrealistic abrasion of these small, suspended grains of little consequence to our broader results.

While the experiments by Attal and Lavé (2009) suggest that the transport dependent abrasion parameter (k) should be greater than 0, they do not provide tight constraints on values for this parameters. While a k of 15 yields an approximate match to the "semi-schematic" diagram of Attal and Lavé (2009) (our Figure 7a), it is unclear whether the slope of their transport-dependent curve has a firm quantitative basis. Given these loose constraints, we explore the sensitivity of downstream volumetric loss of coarse CC source material to plausible values. As we increase k, predicted loss of coarse source material increases (Figure 6). In all cases, this coarse sediment volume loss is dominated by the loss of vesicular volcanics. In the most extreme example modeled here (Figure 6i), we predict loss of 70% of the coarse CC sediment source to wash load during 65 km of transport. Increases in the tumbler correction factor result in increases in total volume loss downstream. However, the rate of loss remains gradual even in the case of $4\alpha_t$. In contrast, increases in the transport-dependence of abrasion (k) result in rapid loss of source material volume in the first ~25 km downstream from the source.

5. A Mixing Model for Downstream Changes in Bed Material Lithology Under Different Abrasion Scenarios

Here, we create a simple model for the downstream changes in coarse bed material in the basin, informed by our field observations of source material characteristics and mapped basin lithology. Our model covers the 65 km of the Suiattle from CC to the confluence with the Sauk River downstream (Figure 2a). We begin with the hypothetical case of no bed material abrasion, and use a variety of methods for calculating abrasion that represent hypothetical sampling schemes with increasing levels of complexity in their representation of the sediment heterogeneity and abrasion process (Table 1).

Table 1
Parameters Used in Abrasion Downstream Mixing Model Scenarios

Scenario	Equation	SHRS Sampling Site	Source SHRS Values	C_t	ρ_s Values	k
1	Sternberg (1875)	road bridge	mean volcanic (57.6)	N/A	constant	N/A
2	Sternberg (1875)	road bridge	mean volcanic (57.6)	**4**	constant	N/A
3	Sternberg (1875)	**source**	mean VV (**49.7**) mean NV (**62.5**)	4	constant	N/A
4	Sternberg (1875)	source	**distribution**	4	**distribution**	N/A
5	Attal and Lavé (2009)	source	distribution	4	distribution	**15**
6	Attal and Lavé (2009)	source	distribution	4	distribution	**45**

Note. Bold text indicates a change from the previous scenario.

5.1. Mixing Model in the Absence of Abrasion

We represent the total coarse sediment load to the river as a collection of 10,000 sediment parcels, each with a given lithology and equal starting volume. Out of 10,000 sediment parcels, we assume that 61% enter the Suiattle River at the CC debris fan. This estimate is based on a study of suspended sediment records in the basin (Jaeger et al., 2017). While a bedload-based estimate of the relative magnitudes of sediment contribution to the channel would be preferable, no such data set exists. For the purpose of our simplified mixing model, we treat this sediment contribution as a point-source at 0 km downstream, with a ratio of vesicular to non-vesicular volcanics set to match the ratio found in the CC debris fan (81% vesicular volcanic, 19% non-vesicular volcanic). The downstream additions of sediment parcels, separated out by lithology category, are illustrated in Figure S7 in Supporting Information S1.

Upstream of Chocolate Fan, gravel bar sediment is a mixture of volcanic and non-volcanic clasts (Figure 5a). From the gravel bar just upstream of Chocolate Fan to the first site incising into the fan, the fraction of non-volcanic lithologies decreases from 58% to 4%. From this observation, we infer that 11.6% of the total non-CC sediment supply (represented as 452 of the 3,900 non-CC parcels) comes from the Suiattle basin upstream of the fan. Of that upstream sediment, we know from bar measurements that 24% is vesicular volcanic, 16% is non-vesicular volcanic, and 2% is volcanic breccia. For simplicity, we combine the breccia with the vesicular volcanics in this mixing model.

Over the 65 km downstream from the CC source, we add the remainder of the non-CC sediment. Along the Suiattle, drainage area increases linearly with distance downstream from Chocolate Fan ($R^2 = 0.98$, Figure S8 in Supporting Information S1). Based on this observation, we add a uniform volume of sediment to each model reach downstream, with lithologies informed by general downstream patterns in the mapped units (Figure 2a). Over the first 13 km downstream from the fan, the added basin area (and, we assume, contributed sediment) is on average 49% volcanic. Downstream from that point, the new contributed basin area is 6.5% volcanic. The downstream volcanic sediment primarily comes from channel-adjacent lahar bluffs (Scott & Collins, 2021), deposited at approximately the same time as the formation of the volcanic apron into which Chocolate and Dusty Creeks are incising (Beget, 1982). Thus, we make the assumption that volcanic sediments in these downstream reaches have the same vesicular fraction, strength, and grain size characteristics as the Chocolate/Dusty Creek source material. We assign all non-volcanic lithologies a SHRS of 73, the mean measured value for non-volcanic clasts (standard deviation = 5.4).

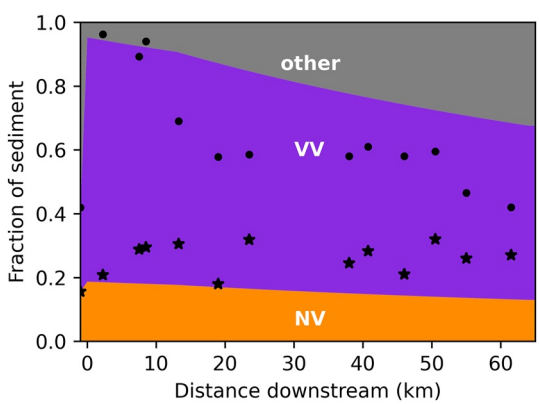

Figure 9. Mixing model of trends in sediment lithology along the Suiattle assuming no bed material abrasion. Measured gravel bar total volcanic fraction (dots) and vesicular volcanic fraction (stars), as in Figure 6, shown in black.

In the absence of bed material abrasion, this mixing model results in consistent overprediction of the volcanic fraction of the bed material downstream from the CC source (Figure 9). Importantly, an abrasion-free model also yields no predicted downstream change in the ratio of vesicular to non-vesicular volcanics, nor a predicted change in the strength of the volcanic bed material.

5.2. Mixing Models With Different Abrasion Scenarios

Many studies that model bed material abrasion rely on bed material samples taken at accessible sites along mainstem channels (for example., Attal et al., 2006; O'Connor et al., 2014; Wickert et al., 2020). For our first, and simplest, hypothetical scenario we calculate bed material abrasion in the Suiattle using the mean SHRS of volcanic clasts (57.6) measured on the gravel bar at the only road that crosses the river (km 46, Figure 2a). Scenario 2 incorporates a tumbler correction factor (C_t) of 4 to account for the fact that barrel tumblers likely underestimate the rate of abrasion in real rivers (Kodama, 1994; Lewin & Brewer, 2002). For the remainder of our hypothetical scenarios (Scenarios 4–6, Table 1), we calculate abrasion using the SHRS of the source material. Scenario 3 uses the mean value of measured vesicular and non-vesicular volcanic SHRS, while scenario 4 incorporates the measured distribution of source material SHRS, predicting downstream abrasion for each of the parcels according to their individual predicted α_t and density (Figure 1). Scenarios 5 and 6 incorporate the transport-dependent abrasion model and a k value of 15 and 45, respectively.

We consider how the result of each abrasion modeling scenario compares to our field observations by comparing the model results to the field observations of total bed material volcanic fraction (Figure 5a), the ratio of vesicular to non-vesicular volcanics, and the volumetric mean SHRS of the coarse (>11 cm) volcanic clasts, calculated as:

$$\overline{\mathrm{SHRS}}_{\mathrm{volc>11cm}} = \frac{\sum \mathrm{SHRS}_i V_i}{\sum V_i} \tag{10}$$

where V_i refers to the volume of parcels of coarse volcanic material at a model distance downstream, and SHRS_i is the SHRS of those coarse volcanic sediment parcels.

The strong relationship between SHRS and abrasion rate (Figure 1a) presents an easy, and tempting, path forward to predicting downstream abrasion from a few simple field measurements. However, we caution that the simplest implementations of this approach are prone to systematically underestimating the magnitude of downstream particle abrasion in several ways. Scenario 1 assumes Sternberg abrasion with a mean abrasion rate derived from our tumbler experiments and SHRS measurements made at the road bridge. This scenario yields calculated loss of just 7.6% of the volume of the coarse CC source material lost to abrasion over 65 km of downstream transport. In the downstream mixing model, this results in 66% volcanic bed material at the outlet, in contrast to our field observation of 42% volcanic at the downstream most site (Figure 10). If we incorporate a C_t of 4 to account for the systematic underprediction of abrasion rates estimated via tumblers (Scenario 2), we calculate that 27% of the source material would be lost over 65 km of transport, yielding a downstream volcanic fraction of 62% in the mixing model. Knowing that the source material is dominated by cobbles and boulders, our abrasion Scenario 1 or 2 might lead us to the incorrect conclusion that selective transport processes outweigh the effects of abrasion in this river, with debris flows leaving large lag deposits of the coarsest material. These first two approaches fail to account for survivorship bias in downstream transport: the weak clasts are preferentially lost to abrasion, and so are underrepresented in the gravel bars downstream.

A third approach to abrasion prediction would be to measure the SHRS of boulders at the source and use the mean vesicular (49.75) and non-vesicular (62.5) volcanic SHRS (and $C_t = 4$) to estimate downstream abrasion (Scenario 3). Importantly, this approach distinguishes between the volcanic clasts on the basis of textural differences. From this approach, we predict substantially more abrasion: loss of 55% of the source material over 65 km of transport, and a downstream bar volcanic fraction of 51% (Figure 10a). However, the loss is very gradual, in contrast to the observation of rapid loss over the first kilometers downstream from the source. Furthermore, the predicted downstream change in the ratio of vesicular and non-vesicular volcanics is far more gradual than the trend we observe in the gravel bars (Figure 10b).

As a final abrasion calculation scenario using the classic Sternberg formulation (Scenario 4), we use the measured distribution of source material SHRS to calculate individual abrasion rates. Scenario 4 yields a similar degree of coarse fraction loss (53%) over the length of the channel. However, the loss is slightly more rapid in the first km of transport, as the weakest grains are preferentially abraded away. While the weakest clast in the source material distribution (SHRS = 24, $\alpha_t = 0.12$) is predicted to lose nearly all of its volume over 65 km of transport, the strongest clast (SHRS = 73.5, $\alpha_t = 0.0001$) is predicted to lose only 0.6% of its volume to abrasion. In this scenario, abrasion is nearly entirely limited to the vesicular fraction of the volcanic source material due to its higher α_t. By specifying the distribution of abrasion rate, rather than simply the mean, we succeed in modeling

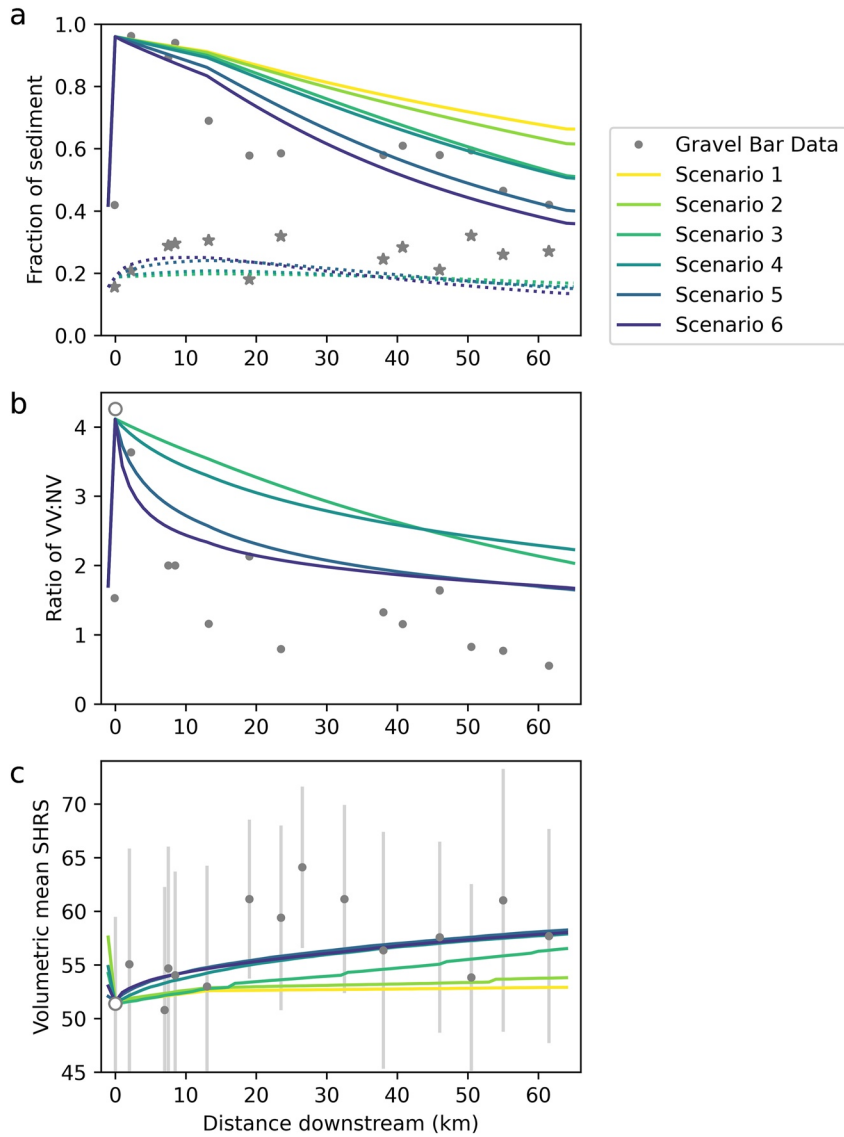

Figure 10. Modeled downstream changes in coarse sediment lithology (colored lines) compared to gravel bar observations (gray points). Solid lines in (a) mark the volumetric fraction of volcanic bed sediment (NV + VV), while dotted lines mark the non-vesicular volcanic fraction. (b) Ratio of VV:NV clasts in the various mixing model scenarios, compared to observed ratios on the bars. (c) Volumetric mean Schmidt Hammer Rock Strength (SHRS) of large (>11 cm) volcanic clasts. Error bars mark the standard deviation of volcanic clast SHRS, as in Figure 4. White dots represent measured values of the source material. Note that scenarios 1 and 2 do not distinguish between VV and NV, and thus are excluded from panel b.

a higher concentration of non-vesicular volcanic grains at sites far downstream (Figure 10b). This finding highlights the importance of characterizing source material heterogeneity. However, Scenario 4 falls short in several ways. First, while the general trend in the vesicular to non-vesicular ratio is correct, the magnitude of decrease is insufficient to match field data (Figure 10). Second, the field data shows rapid loss of volcanic fraction in the first kilometers downstream from the CC source and high volcanic fraction upper reaches of the Suiattle. The downstream changes in Scenario 4 are comparatively gradual. Third, the volumetric mean SHRS of the coarse (>11 cm) volcanic grains in the model (Figure 10c) increases only slightly and gradually downstream, far from the rapid increase seen in our field data. With these shortcomings in mind, we turn to a more sophisticated model for bed material abrasion processes.

Building on the abrasion scenarios and mixing model outlined in above, we calculate volumetric loss of the coarse bed material using the transport-dependent abrasion model and a k value of 15 (Scenario 5) and 45 (Scenario 6,

Table 1). The incorporation of transport-dependent abrasion results in a rapid loss of CC source material volume in the first 20 km, followed by a gradual decline in the lower river. This rapid loss of coarse material to abrasion is restricted almost entirely to weaker vesicular volcanic grains, resulting in rapid bed material strengthening (Figure 10c) and change in the ratio of vesicular to non-vesicular volcanics that is not present in the scenarios that simply model abrasion as a function of transport distance (Figure 10b).

Our model for bed material abrasion falls short in two respects. First, in all model scenarios, we predict a lower rate and magnitude of volcanic bed material strengthening (Figure 10c) than we observe in the field. Over the first 19 km downstream from CC, we measured a change in SHRS from 51 to >60. Even our highest-abrasion end member scenario (Scenario 6) predicts a lesser degree of clast strengthening, reaching SHRS = 56 over the first 19 km. Despite this underprediction of the magnitude of downstream strengthening, the transport-dependent scenarios (5 and 6) do a substantially better job of matching the field data than the classic Sternberg (1875) scenarios. Both the model and the measurements show rapid bed material strengthening over the first 25 km downstream from the sediment source, followed by more gradual change. Second, while the transport-dependent abrasion scenarios successfully produce an abrupt initial loss in weak vesicular volcanics and associated decrease in the ratio of vesicular to non-vesicular volcanics (Figure 6), the magnitude of these changes remains insufficient to explain the observed trends in gravel bar lithology (Figures 10a and 10b). Further increasing the degree of transport dependence (k) or tumbler correction factor (C_t), is not well supported by the findings of Attal and Lavé (2009) and Lewin and Brewer (2002), respectively. Below, we consider some potential abrasion and transport processes that are likely required to explain our observations.

6. Discussion

6.1. Need for Advances in Theory and Modeling of Bed Material Abrasion

Comparing our field observations to models for bed material abrasion in the Suiattle, we find that the classic exponential model for mass loss (Sternberg, 1875) is unable to reproduce the observed downstream patterns in lithology and rock strength, even when accounting for the heterogeneity in source material strength (Scenario 4, Figure 10). While the transport-dependent abrasion model successfully produces an abrupt initial loss in weak vesicular volcanics (Figure 10a and Figure 6), associated decrease in the ratio of vesicular to non-vesicular volcanics (Figure 10b), and strengthening of the volcanic bed material, the magnitude of these changes remains insufficient to tightly match our observations of downstream lithologic change and clast strengthening.

While transport-dependent abrasion will tend to enhance the downstream loss of finer and lower-density particles, there are two potentially important abrasion processes that likely enhance the abrasion of coarse particles that we have not represented. First, Attal and Lavé (2009) noted that larger grains tend to abrade at a higher rate, due in part to an increase in fragmentation as grain size increases. This is represented in our model as an increase in α with D in Equation 6. In this representation, α is insensitive to grain size below $\tau^*/\tau_{*_c} = 3.3$. The experiments by Attal and Lavé (2009) are inconclusive as to the sensitivity of abrasion rate to grain size at low transport rates. Lacking more quantitative constraints on the relationship between lithologic strength, grain size, and baseline abrasion, we have not attempted to include this in our model. However, this grain size dependence may be important in the Suiattle, with its poorly sorted source grain mixture.

Second, and perhaps most importantly, we have not accounted for size-selective transport in our modeling. The CC debris flow material, the major sediment source in the basin, ranges in size from silt to >1 m boulders. Thus, size-selective transport is almost certainly a major control on the residence time of sediment in the basin. Large, nearly immobile grains will abrade as they jostle in place (Schumm & Stevens, 1973) and are impacted by passing mobile grains (Prancevic et al., 2020). Thus, large but weak grains are especially prone to the effects of in-place abrasion. While these components of the abrasion process have been long recognized, quantitative representations for the process have yet to be refined. This sedentary abrasion will increase the mass loss per kilometer of transport for large grains that transport slowly, resulting in mass loss that is rapid in space but slow in time when compared to the abrasion of small, highly mobile grains. Because lithology acts as a first-order control on baseline abrasion rate (Lewin & Brewer, 2002), we predict that in-place abrasion would result in greater loss of vesicular relative to non-vesicular volcanics, despite their lower densities and therefore higher transport rates. Both of these abrasion mechanisms neglected in our model have the potential to help resolve our failure to fully reproduce

the observed magnitude of downstream clast strengthening and the rapid decrease in the volcanic fraction of the bed material in the first kilometers downstream from the sediment source at CC.

Historically, much of the literature on bed material abrasion has focused on comparing its relative importance to size-selective transport in controlling downstream fining. Here, our focus has been on abrasion-set controls on downstream coarse sediment flux and lithologic mixtures, explicitly omitting consideration of downstream fining. However, it is possible that size-selective transport could play a role in the downstream evolution of clast strength and lithologic mixtures, and that the discrepancy between our modeling and field observations could be explained by incorporating size-selective transport.

Our findings have potentially intriguing implications for bed material morphodynamics of heterogeneous material. The low density, weak grains shrink in diameter rapidly downstream due to their high baseline abrasion rate and the enhanced transport-dependent abrasion promoted by the low clast density. The downstream reduction in size further enhances both transport rate and transport-dependent abrasion, suggesting a transport feedback with abrasion in low-strength clasts. These effects have intriguing implications for sediment pulse transfer in weak or heterogeneous sediments. Modeling work to address these questions (and in-place abrasion) would require advances in our quantitative description of abrasion, informed by detailed field or laboratory experiments, and modeled with a Lagrangian morphodynamic model that individually tracks the downstream evolution of parcels of sediment of varying abrasion rate, density, and size (e.g., Czuba, 2018; Pfeiffer et al., 2020).

6.2. The Importance of Heterogeneity

Geomorphologists are likely to treat sediment from a single mapped rock unit as a uniform lithology, assuming a single abrasion rate (e.g., O'Connor et al., 2014). Our findings, particularly the downstream increase in clast strength and preferential loss of vesicular volcanics, demonstrate the potential peril of this approach. Stratovolcanoes, such as the source zone of our study area, are particularly prone to the problem of easily underestimated bed material abrasion, given the wide range of tephra rock strength and clast density. Predicting abrasion rate is important in these settings because the downstream hazards of coarse sediment (e.g., increased flooding due to channel aggradation (Slater et al., 2015)) are different from downstream hazards associated with the fine sediment products of abrasion (e.g., habitat degradation (Greig et al., 2005)).

While some lithologies likely produce sediment of uniform strength, heterogeneous abrasion rates are not limited to stratovolcanoes. Some sedimentary rock units and metamorphic mélanges are quite heterogeneous as well, with substantial variability in rock strength at the outcrop or bedform scale (Bernard et al., 2019). In a study of sediment pulse transfer in the Navarro River of Northern California, Sutherland et al. (2002) found an apparent reduction in α over time during their abrasion experiments of landslide deposits consisting of a mix of sandstone, siltstone, and mudstone. This can be explained by a preferential loss of weak clasts early in the experiment. Their results mirror our finding of rapid downstream clast strengthening in the Suiattle. We are not the first to recognize the role of survivorship bias in sediment abrasion (Adams, 1979), but the importance of this phenomena seems to be frequently overlooked.

7. Conclusion

Our site, with its heterogeneous source material from a localized headwater source, combined with our SHRS method to quantify the relative abrasion potential of source and bed material, provides a rich data set with which to test existing understanding of bed material abrasion processes. The standard exponential model for downstream abrasion fails to reproduce observed downstream patterns in lithology and clast strength in the Suiattle, even when accounting for the heterogeneity of source material strength and systematic underestimate of abrasion rates by tumbler experiments. Incorporating transport-dependent abrasion into our model greatly improves results, though the rate of loss of volcanic bed material and the magnitude of downstream strengthening remain lower in our models than we measure in the field. These shortcoming hint at further complexities in the abrasion process for which we presently lack quantitative process descriptions.

Data Availability Statement

The field measurements of grain size, lithology, and SHRS, as well as the abrasion tumbler experimental results, are published online at https://doi.org/10.5281/zenodo.6522210 (Pfeiffer, 2022), available via Creative Commons Attribution 4.0 International Public License.

Acknowledgments
We thank Selina Davila Olivera, Jaycob Davies, Riley Keister, Vivien McNett, Stephen Novak, and Ana Zissou for assistance in the field, and Gabe Gordon, JoJo Mangano, and Jim O'Connor for use of the rock tumbler. We thank Erkan Istanbulluoglu, Brian Collins, Dan Scott, Scott Anderson, and the UW PREEVENTS Group for feedback that helped guide this work. Funding for was provided by Western Washington University, the Quaternary Research Center at the University of Washington, an NCED II Postdoctoral Fellowship (to A. Pfeiffer), and NSF PREEVENTS program (ICER 1663859, to E. Istanbulluoglu).

References

Adams, J. (1979). Wear of unsound pebbles in river headwaters. *Science*, *203*, 171–172. https://doi.org/10.1126/science.203.4376.171

Anderson, S. W., & Konrad, C. P. (2019). Downstream-propagating channel responses to decadal-scale climate variability in a glaciated River basin. *Journal of Geophysical Research: Earth Surface*, *124*, 902–919. https://doi.org/10.1029/2018JF004734

Attal, M., & Lavé, J. (2006). Changes of bedload characteristics along the Marsyandi River (central Nepal): Implications for understanding hillslope sediment supply, sediment load evolution along. *Tectonics, climate, and landscape evolution*, *2398*, 143–171. https://doi.org/10.1130/2006.2398(09)

Attal, M., & Lavé, J. (2009). Pebble abrasion during fluvial transport: Experimental results and implications for the evolution of the sediment load along rivers. *Journal of Geophysical Research*, *114*, 1–22. https://doi.org/10.1029/2009JF001328

Attal, M., Lavé, J., & Masson, J.-P. (2006). New facility to study river abrasion processes. *Journal of Hydraulic Engineering*, *132*, 624–628.

Beget, J. E. (1982). *Postglacial volcanic deposits at Glacier Peak, Washington, and potential hazards from future eruptions*. Open-File Report 82-830. Geological Survey.

Bernard, T., Sinclair, H. D., Gailleton, B., Mudd, S. M., & Ford, M. (2019). Lithological control on the post-orogenic topography and erosion history of the Pyrenees. *Earth and Planetary Science Letters*, *518*, 53–66. https://doi.org/10.1016/j.epsl.2019.04.034

Bradley, W. C. (1970). Effect of weathering on abrasion of granitic gravel, Colorado river (Texas). *The Geological Society of America Bulletin*, *81*(1), 61–80. https://doi.org/10.1130/0016-7606(1970)81[61:EOWOAO]2.0.CO;2

Brierley, G. J., & Hickin, E. J. (1991). Channel planform as a non-controlling factor in fluvial sedimentology: The case of the squamish river floodplain, British columbia. *Sedimentary Geology*, *75*, 67–83. https://doi.org/10.1016/0037-0738(91)90051-E

Bunte, K., & Abt, S. R. (2001). Sampling surface and subsurface particle-size distributions in wadable gravel- and cobble-bed streams for analyses in sediment transport, hydraulics, and streambed monitoring. In *General technical report RMRS-GTR-74*. USDA Forest Service.

Czuba, J. A. (2018). A Lagrangian framework for exploring complexities of mixed-size sediment transport in gravel-bedded river networks. *Geomorphology*, *321*, 146–152. https://doi.org/10.1016/j.geomorph.2018.08.031

Czuba, J. A., Magirl, C. S., Czuba, C. R., Grossman, E. E., Curran, C. A., Gendaszek, A. S., & Dinicola, R. S. (2011). *Sediment load from major rivers into puget sound and its adjacent waters*. U.S. Geological Survey Fact Sheet 2011–3083. U.S. Geological Survey.

Daubrée, A. (1879). *Études synthétiques de Géologie expérimentale*. Dunod.

Demirdag, S., Yavuz, H., & Altindag, R. (2009). The effect of sample size on Schmidt rebound hardness value of rocks. *International Journal of Rock Mechanics and Mining Sciences*, *46*, 725–730. https://doi.org/10.1016/j.ijrmms.2008.09.004

Dingle, E. H., Attal, M., & Sinclair, H. D. (2017). Abrasion-set limits on Himalayan gravel flux. *Nature*, *544*, 471–474. https://doi.org/10.1038/nature22039

Domokos, G., Jerolmack, D. J., Sipos, A. Á., & Török, Á. (2014). *How river rocks round: Resolving the shape-size paradox*. In V. Magar (Ed.) (Vol. 9). e88657. PLoS ONE. https://doi.org/10.1371/journal.pone.0088657

Duvall, A., Kirby, E., & Burbank, D. (2004). Tectonic and lithologic controls on bedrock channel profiles and processes in coastal California. *Journal of Geophysical Research*, *109*. https://doi.org/10.1029/2003JF000086

East, A. E., Pess, G. R., Bountry, J. A., Magirl, C. S., Ritchie, A. C., Logan, J. B., et al. (2015). Large-scale dam removal on the Elwha River, Washington, USA: River channel and floodplain geomorphic change. *Geomorphology*, *228*, 765–786. https://doi.org/10.1016/j.geomorph.2014.08.028

Ferguson, R., Hoey, T., Wathen, S., & Werritty, A. (1996). Field evidence for rapid downstream fining of river gravels through selective transport. *Geology*, *24*, 179–182. https://doi.org/10.1130/0091-7613(1996)024<0179:FEFRDF>2.3.CO;2

Ford, A. B. (1959). *Geology and petrology of the Glacier Peak quadrangle, northern Cascades, Washington, PhD thesis*. University of Washington.

Gasparini, N. M., Tucker, G. E., & Bras, R. L. (2004). Network-scale dynamics of grain-size sorting: Implications for downstream fining, stream-profile concavity, and drainage basin morphology. *Earth Surface Processes and Landforms*, *29*, 401–421. https://doi.org/10.1002/esp.1031

Greig, S. M., Sear, D. A., & Carling, P. A. (2005). The impact of fine sediment accumulation on the survival of incubating salmon progeny: Implications for sediment management. *The Science of the Total Environment*, *344*, 241–258. https://doi.org/10.1016/j.scitotenv.2005.02.010

Hoey, T. B., & Ferguson, R. (1994). Numerical simulation of downstream fining by selective transport in gravel bed rivers: Model development and illustration. *Water Resources Research*, *30*, 2251–2260. https://doi.org/10.1029/94WR00556

Huddart, D. (1994). Rock-type controls on downstream changes in clast parameters in sandur systems in southeast Iceland. *SEPM Journal of Sedimentary Research*, *64A*. https://doi.org/10.1306/D4267D61-2B26-11D7-8648000102C1865D

Jaeger, K. L., Curran, C. A., Anderson, S. W., Morris, S. T., Moran, P. W., & Reams, K. A. (2017). Suspended sediment, turbidity, and stream water temperature in the Sauk River Basin, Western Washington, water years 2012–16. U.S. Geological Survey Scientific Investigations Report 2017–5113, 47. https://doi.org/10.3133/sir20175113

Kahraman, S., & Gunaydin, O. (2007). Empirical methods to predict the abrasion resistance of rock aggregates. *Bulletin of Engineering Geology and the Environment*, *66*, 449–455. https://doi.org/10.1007/s10064-007-0093-2

Kodama, Y. (1994). Experimental study of abrasion and its role in producing downstream fining in gravel-bed rivers. *Journal of Sedimentary Research*, *64*, 76–85. https://doi.org/10.2110/jsr.64.76

Kuenen, H. (1956). Experimental abrasion of pebbles: 2. Rolling by current. *The Journal of Geology*, *64*, 336–368. https://doi.org/10.1086/626370

Lewin, J., & Brewer, P. A. (2002). Laboratory simulation of clast abrasion. *Earth Surface Processes and Landforms: The Journal of the British Geomorphological Research Group*, *27*, 145–164.

Miller, K. L., Szabó, T., Jerolmack, D. J., & Domokos, G. (2014). Quantifying the significance of abrasion and selective transport for downstream fluvial grain size evolution. *Journal of Geophysical Research: Earth Surface*, *119*, 2412–2429. https://doi.org/10.1002/2014JF003156

Mueller, E. R., Smith, M. E., & Pitlick, J. (2016). Lithology-controlled evolution of stream bed sediment and basin-scale sediment yields in adjacent mountain watersheds, Idaho, USA. *Earth Surface Processes and Landforms*, *1883*, 1869–1883. https://doi.org/10.1002/esp.3955

Murphy, B. P., Johnson, J. P. L., Gasparini, N. M., & Sklar, L. S. (2016). Chemical weathering as a mechanism for the climatic control of bedrock river incision. *Nature*, *532*, 223–227. https://doi.org/10.1038/nature17449

O'Connor, J. E., Mangano, J. F., Anderson, S. W., Wallick, J. R., Jones, K. L., & Keith, M. K. (2014). Geologic and physiographic controls on bed-material yield, transport, and channel morphology for alluvial and bedrock rivers, Western Oregon. *Bulletin of the Geological Society of America*, *126*, 377–397. https://doi.org/10.1130/B30831.1

Pfeiffer, A. M. (2022). *River bed sediment and debris flow deposit lithology and Schmidt Hammer Rock Strength dataset*. [online] Retrieved from https://zenodo.org/record/6522210. Accessed 6 May 2022.

Pfeiffer, A. M., Barnhart, K. R., Czuba, J. A., & Hutton, E. W. H. (2020). NetworkSedimentTransporter: A landlab submodule for bed material transport through river networks. *Journal of Open Source Software*, *5*, 2341. https://doi.org/10.21105/joss.02341

Pfeiffer, A. M., Finnegan, N. J., & Willenbring, J. K. (2017). Sediment supply controls equilibrium channel geometry in Gravel Rivers. *Proceedings of the National Academy of Sciences*, *114*, 3346–3351. https://doi.org/10.1073/pnas.1612907114

Prancevic, J., Sklar, L. S., & Dietrich, W. E. (2020). Modeling how rivers digest boulders: Long residence times and coarse riverbed surfaces lead to preferential wear of boulders through in-place abrasion. *Presented at the American Geophysical Union Fall Meeting*. Online. EP007-05.

Richardson, D. (1968). *Glacier outburst floods in the Pacific Northwest. U.S. Geological survey professional paper 600-D*. US Geological Survey.

Schumm, S. A., & Stevens, M. A. (1973). Abrasion in place: A mechanism for rounding and size reduction of coarse sediments in rivers. *Geology*, *1*, 37–40.

Scott, D. N., & Collins, B. D. (2021). Frequent mass movements from glacial and lahar terraces, controlled by both hillslope characteristics and fluvial erosion, are an important sediment source to puget sound rivers. *Water Resources Research*, *57*. https://doi.org/10.1029/2020WR028389

Sklar, L. S., & Dietrich, W. E. (2004). A mechanistic model for river incision into bedrock by saltating bed load. *Water Resources Research*, *40*. https://doi.org/10.1029/2003WR002496

Slater, L. J., Singer, M. B., & Kirchner, J. W. (2015). Hydrologic versus geomorphic drivers of trends in flood hazard. *Geophysical Research Letters*, *42*, 370–376. https://doi.org/10.1002/2014GL062482

Slaughter, S. L. (2004). *The 1938 chocolate glacier debris flow*. Glacier Peak VolcanoCentral Washington University.

Sternberg, H. (1875). Untersuchungen uber langen-und querprofil geschiebefuhrender flusse. *Zeitshrift fur Bauwesen*, *25*, 483–506.

Sutherland, D. G., Ball, M. H., Hilton, S. J., & Lisle, T. E. (2002). Evolution of a landslide-induced sediment wave in the Navarro River, California. *Bulletin of the Geological Society of America*, *114*, 1036–1048. https://doi.org/10.1130/0016-7606(2002)114<1036:EOALIS>2.0.CO;2

Wickert, A. D., Schildgen, T. F., Tofelde, S., Savi, S., Rojo, Y., Fleagle, S., et al. (2020). Self-consistently matching sediment supply, water discharge, and channel slope: Lane's balance at the catchment scale. *Presented at the AGU fall meeting abstracts*. Online. EP014-06.